

Highlights

Cooperative Adaptive Cruise Platoon Controller Design Considering Head-to-tail String Stability and Control Switching

Hao Wang,Tiancheng Ruan,Linjie Zhou,YuXuan Hou,Rui Jiang

- Adopted head-to-tail string stability analyses for controller design.
- Proposed a CACC platoon control which is adaptable for any platoon size.
- Applied YK parameterization to ensure stable interpolation between controllers.
- Parameters of the lower control level of vehicle is calibrated by field tests.
- Explored a gain-scheduling scheme of CACC platoon to make it stable and effective.

Cooperative Adaptive Cruise Platoon Controller Design Considering Head-to-tail String Stability and Control Switching

Hao Wang^{a,b,c,*}, Tiancheng Ruan^{a,b,c}, Linjie Zhou^{a,b,c}, YuXuan Hou^{a,b,c} and Rui Jiang^{d,*}

^aJiangsu Key Laboratory of Urban ITS, Southeast University, 2 Si Pai Lou, Nanjing, 210096, P.R. China

^bJiangsu Province Collaborative Innovation Center of Modern Urban Traffic Technologies, 2 Si Pai Lou, Nanjing, 210096, P.R. China

^cSchool of Transportation, Southeast University, 2 Si Pai Lou, Nanjing, 210096, P.R. China

^dKey Laboratory of Transport Industry of Big Data Application Technologies for Comprehensive Transport, Ministry of Transport, Beijing Jiaotong University, Beijing, 100044, P.R. China

ARTICLE INFO

Keywords:

Cooperative adaptive cruise control
Platoon control
Head-to-tail string stability
Switching control

ABSTRACT

With the development of Cooperative Adaptive Cruise Control (CACC) technology, CACC Market Penetration Rate (MPR) is expected to increase rapidly in the near future, which will result in more CACC platoons. Controller design seeking strict string stability is unable to take full advantage of CACC platoons which can maintain head-to-tail stability with a smaller desired time gap. This paper first proposed a novel CACC controller design mode—Cooperative Adaptive Cruise Platoon Control (CACPC)—that takes the CACC platoon as the control object to further use CACC technology. Secondly, an control switching method, Youla-Kučera (YK) parameterization, was adopted to ensure stability while switching the two control modes under different platoon sizes. Finally, numerical analyses and simulations were conducted to explore the effectiveness of CACPC on dynamic performance. It is found that YK parameterization can significantly suppress the perturbation caused by the switching of control mode and maintain stability during the switching.

1. Introduction

To maintain safety, mobility, and environmental sustainability as transportation systems develop rapidly, Connected Autonomous Vehicle (CAV) technology has burgeoned and attracted considerable attention in the past decade. The connectivity and automation of the vehicle have been significantly improved. Vehicle-to-Infrastructure (V2I) communication technology guarantees partial or full automation with the help of in-vehicle sensors, and Vehicle-to-Vehicle (V2V) communication technology enables communication and cooperation between vehicles (Wang et al., 2019; Ploeg et al., 2011; Zhou et al., 2021).

The most typical application of V2V communication is Cooperative Adaptive Cruise Control (CACC). A vehicle controlled by this type of system automatically follows the preceding vehicles. Simulation results and field experiments reveal that, compared with traditional vehicles, cooperatively controlled CAVs can maintain a shorter time headway between vehicles. Therefore, consecutively connected vehicles can form a platoon-based driving mode through Cellular vehicle-to-everything (C-V2X) communication to improve traffic efficiency (Gong and Du, 2018; Wang et al., 2020).

According to the literature (Qin et al., 2018; Ruan et al., 2021), standard car-following models should guarantee local stability, which means perturbations will gradually disappear over time. Furthermore, most CACC controllers are designed for maintaining the strict string stability of CACC platoon (Wang, 2018; Sun et al., 2018; Ploeg et al., 2013) which will inevitably lead to much redundancy hence the need for optimization.

Moreover, it will take a long time for CACC MPR to grow due to the immaturity of CACC technology, as the CACC MPR is projected to be only 24.8% in 2045, according to the latest research (Bansal and Kockelman, 2017). Moreover, since a small amount of CACCs cannot guarantee that communication functions properly, most CACCs will degrade into Adaptive Cruise Controls (ACCs) (Ruan et al., 2021; Qin et al., 2018). Therefore, the performance of short CACC platoon is still worth studying.

In order to leverage the benefit of CACCs, this paper proposed a new decentralized control mode named Cooperative Adaptive Cruise Platoon Control (CACPC) that has taken the CACC platoon as the control object instead

*Corresponding author

✉ haowang@seu.edu.cn (H. Wang); ruantiancheng@seu.edu.cn (T. Ruan); 220193107@seu.edu.cn (L. Zhou); NOTEVENWRONG@outlook.com (Y. Hou); jiangrui@bjtu.edu.cn (R. Jiang)

ORCID(s):

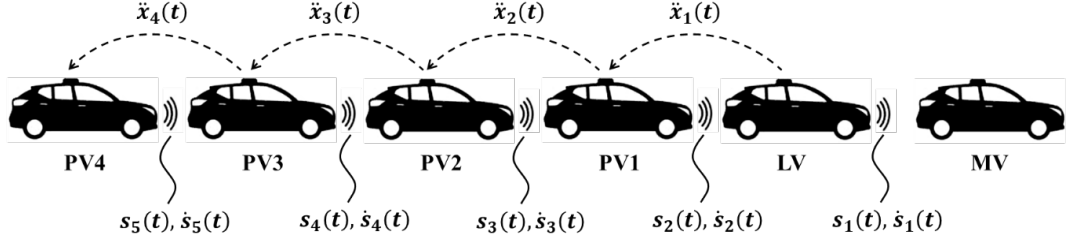


Figure 1: Schematic of CACC platoon.

of a single vehicle. Firstly, we explored the combination of margin stable desired time gap under different platoon sizes using string stability analyses. Secondly, Youla-Kučera (YK) parameterization was adopted to guarantee smoothness and stability in the switching of control mode. Thirdly, a tuning function was proposed to ensure the application under different platoon sizes. Finally, the effectiveness of CACPC on dynamic performance was explored.

The rest of this paper is organized as follows. Section 2 introduces the CACC system setup, control objectives, and control structure studied in this paper. Section 3 proposes the primary methodology includes string stability analyses and YK parameterization. The theoretical results are presented in Section 4. Section 5 validates the theoretical results and explores the impact of CACPC. The conclusion is summarized in Section 6.

2. Problem Formulation

This section mainly introduces the background knowledge of the problems studied in this paper from three perspectives: CACC system setup, control objectives, and control structure.

2.1. CACC System Setup

Fig. 1 shows a schematic of the CACC platoon, where $s_i(t), \dot{s}_i(t)$ indicate the relative gap and relative velocity that CACC obtained through the onboard sensor, and $\ddot{x}_{i-1}(t)$ is the acceleration of the predecessor vehicle obtained through V2V communication.

The CACC design is based on a standard ACC system equipped with a communication module. A CACC platoon can be divided into an Leader Vehicle (LV) and S-1 Platoon vehicles (PV)s based on the communication ability of the predecessor vehicle, where S denotes the maximum size of a CACC platoon. Notice that we think the CACC platoon can not be infinitely long due to the limitation of unreliable communication environment and we assume the maximum platoon size is the platoon size which can keep communication function well. The LVs degrades to ACCs functionally because the predecessor vehicle is ACC or MV and cannot communicate, while the communication module of PVs is functioning (Dey et al., 2015; Navas and Milanés, 2019).

Considering the feasibility of implementation, the controller used in this paper is a decentralized controller instead of a centralized one. The specific information flow topology (IFT) is predecessor following (PF) which means CACCs only communicate with the nearest predecessor to gain further information in advance. As for spacing policy, Constant Time Gap (CTG), including a constant part and a velocity-dependent part, is applied due to its widespread use.

2.2. String stability

We have considered the nuances in different definitions of string stability in the literature. In this paper, the "head-to-tail" string stability is adopted. Namely, the perturbation will not be amplified during upstream propagation (Qin and Wang, 2021; Montanino et al., 2021; Jin and Orosz, 2014; Zhou et al., 2020; Wang, 2018), i.e., from vehicle LV to vehicle PV4 (see Fig. 1). As for specific spacing policy, the error $e_i(t)$ between the desired and actual inter-vehicle gap is frequently considered in CTG to prevent collisions.

In this paper, the head-to-tail string stability of the CACC platoon is studied as a whole instead of analyzing each CACC in the platoon. To facilitate the analysis and focus on the amplification of perturbation, a frequency-domain approach is adopted to obtain a necessary and sufficient condition for the head-to-tail string stability of the CACC platoon, which will provide support for designing CACPC.

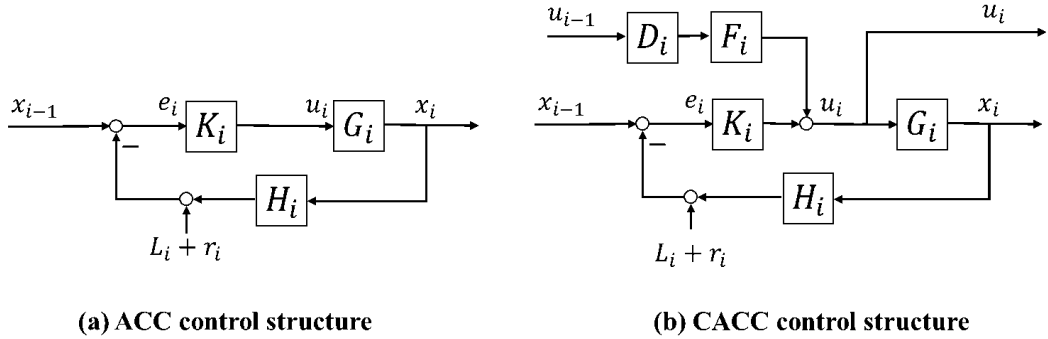


Figure 2: Control structure of ACC and CACC: (a) ACC; (b) CACC.

2.3. Control Structure

The CACC design is based on a standard ACC system and applies the most commonly used CTG policy. In this subsection, the control structures of the ACC and CACC system are discussed respectively in order to study the subsequent design of CACPC.

It is assumed that each CACC is equipped with i) an on-board radar responsible for collision detection via measuring the gap distance between any two consecutive vehicles, ii) a built-in GPS sensor for measuring the vehicular longitudinal position information, iii) a wireless on-board unit for communicating information of interest with its proximal vehicles via the C-V2X communication, iv) an upper-level controller for calculating the desired longitudinal acceleration based on the parameters obtained, and v) a lower-level controller for determining the throttle and brake actuator inputs so as to track the desired acceleration. Such an assumption is reasonable as the sensing, communication, and actuation units requested above are available in modern CAVs, and thus do not require specific changes in the existing vehicle configuration. Note that the on-board radar only functions when the CACC degrades to the ACC if communication is unavailable or malfunctioning since more accurate information can be obtained faster via communication.

Moreover, we remark that this paper only focus on the homogeneous CACCs where CACCs have same control structure and controller parameters.

2.3.1. ACC Control Structure

The primary control object of the ACC system is to maintain the desired gap from the preceding vehicle $s_{d,i}(t) = r_i + L_i + h_i \dot{x}_i(t)$, including a velocity-dependent part and a constant part, where L_i represents the vehicle length, r_i is the standstill distance and h_i is the desired time gap of vehicle i . Using the onboard sensor, the relative gap $s_i(t) = x_{i-1}(t) - x_i(t)$ and relative velocity $\dot{s}_i(t)$ are measured. In a standard ACC system, the feedback controller controls the error $e_i(t) = s_i(t) - s_{d,i}(t)$ between the desire gap and relative gap.

The ACC control structure is schematically depicted in Fig. 2 (a).

As shown in Fig. 2 (a), the ACC control structure is represented as a system construction drawing with vehicle position as input and output. The model $K_i(s)$ is the ACC feedback gain, which can be given as:

$$K_i(s) = k_p + k_d s, \quad (1)$$

where k_p is error gain and k_d is error speed gain, the specific parameter setting is based on previous research (Milanés and Shladover, 2014; Milanés et al., 2013).

The model $G_i(s)$ represents a lower level controller longitudinal vehicle dynamics, where the input $u_i(t)$ of $G_i(s)$ is the desired acceleration derived from $K_i(s)$ and the output $x_i(t)$ is the output position based on the control loop to track desired acceleration through actuation of the throttle and brake system. The linear transfer function of $G_i(s)$ can be represented by (Ploeg et al., 2013):

$$G_i(s) = \frac{k_G}{s^2 (\tau_i s + 1)} e^{-\phi_i s}, \quad (2)$$

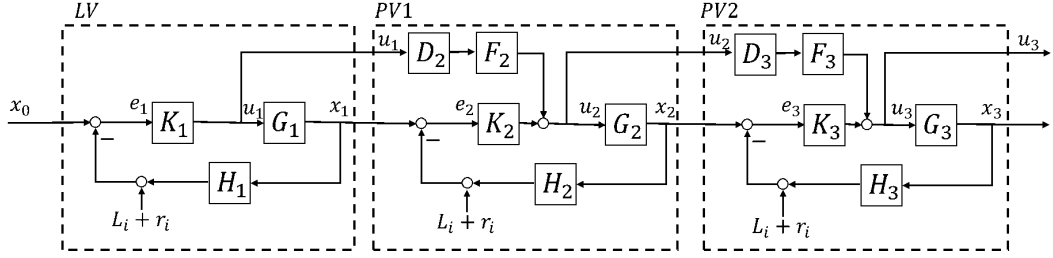


Figure 3: CACPC structure.

where $\tau_i^{-1} = \omega_{bw,i} L_i$ is the closed-loop bandwidth, k_G is the model gain and ϕ_i is the time delay of vehicle actuator and communication, the specific parameter setting is shown in Table. 1.

Model $H_i(s)$ is the ACC feedback gain, which can be given as:

$$H_i(s) = 1 + h_i s, \quad (3)$$

where h_i is the desired time gap of vehicle i.

The closed-loop transfer function of ACC system in the frequency domain is as follows:

$$J_{i,ACC}(s) = \frac{X_i(s)}{X_{i-1}(s)} = \frac{G_i(s)K_i(s)}{1 + H_i(s)G_i(s)K_i(s)}, \quad (4)$$

where $X_i(s)$ is the Laplace transform of $x_i(t)$.

2.3.2. CACC Control Structure

As discussed above, the CACC controller is equipped with a communication module that extended the standard ACC feedback controller. The specific control structure is schematically depicted in Fig. 2 (b).

For simplicity, the definitions of model $H_i(s), G_i(s), K_i(s)$ in system construction drawing are omitted because they are the same as those in Section 2.3.1. The acceleration $\dot{x}_{i-1}(t)$ of predecessor vehicle obtained through V2V communication is used as a feedforward control signal through the feedforward filter $F_i(s)$ and the communication delay model $D_i(s)$.

The model $D_i(s)$ is directly related to the constant communication delay θ_i , which can be expressed as:

$$D_i(s) = e^{-\theta_i s}, \quad (5)$$

where θ_i represents the constant communication delay. The specific parameter setting is according to previous researches (Navas et al., 2016; Zhang et al., 2020).

The model $F_i(s)$ is the communication feedforward filter which can be given as:

$$F_i(s) = (H_i(s)G_i(s))^{-1}. \quad (6)$$

The closed-loop transfer function of CACC system in the frequency domain is as follows:

$$J_{i,CACC}(s) = \frac{X_i(s)}{X_{i-1}(s)} = \frac{(K_i(s) + D_i(s)F_i(s)) G_i(s)}{1 + H_i(s)G_i(s)K_i(s)}. \quad (7)$$

2.3.3. CACPC structure

As the control system for the controller design in this paper, the CACC platoon is designated as the primary control unit for string stability analyses. We can couple the control structure of ACC and CACC by merging the inner and outer signals, thus establishing the structure of CACPC. The specific structure of the CACPC is schematically depicted in Fig. 3.

For simplicity, the definitions of model $H_i(s), G_i(s), K_i(s)$ and $D_i(s)$ in system construction drawing are omitted because they are the same as those in Section 2.3.1 and 2.3.2.

The closed-loop transfer function of CACPC system in the frequency domain is as follows:

$$\mathcal{J}_{\text{platoon}}(s) = \frac{X_n(s)}{X_0(s)} = \frac{X_n(s)}{X_{n-1}(s)} \frac{X_{n-1}(s)}{X_{n-2}(s)} \cdots \frac{X_1(s)}{X_0(s)} = \mathcal{J}_{1,ACC}(s) \prod_{i=2}^n \mathcal{J}_{i,CACC}(s), \quad (8)$$

where n denotes the platoon size.

3. Methodology

In this section, the primary methodology applied in this paper is introduced, including the transfer function method for string stability analyses and the YK parameterization for controller switching.

3.1. String stability analyses

Laplace transform is a classic method to explore string stability in a direct and precise manner. Moreover, it has been adopted in several researches (Orosz et al., 2011; Montanino and Punzo, 2021; Feng et al., 2019). Therefore, the head-to-tail string stability analyses of this paper are conducted based on the Laplace transform. The relationship of the perturbation propagating through CACC platoon in the frequency domain is:

$$\mathcal{J}_{\text{platoon}}(s) = \frac{X_n(s)}{X_0(s)}. \quad (9)$$

According to the definition of string stability, a sufficient and necessary conservative condition for string stability can be derived according to the \mathcal{L}_∞ norm:

$$\|x_n(t)\|_{\mathcal{L}_\infty} \leq \|x_0(t)\|_{\mathcal{L}_\infty} \quad (10)$$

where $x_n(t)$ and $x_0(t)$ are the inverse Laplace transformation of $X_n(s)$ and $X_0(s)$, respectively; $\|\cdot\|_{\mathcal{L}_\infty}$ is the \mathcal{L}_∞ norm, which deals with the deal with the peak of perturbations.

Moreover, according to the relationship $\|g\|_1 = \sup_{x \in L_\infty} \frac{\|y\|_{\mathcal{L}_\infty}}{\|x\|_{\mathcal{L}_\infty}}$ Equation(10) can be replaced as:

$$\|j(t)\|_1 \leq 1 \quad (11)$$

where $j(t)$ denotes the impulse response of $\mathcal{J}_{\text{platoon}}(s)$.

Furthermore, the Equation(11) can be replaced by the following two conditions (Swaroop, 1994):

$$\|\mathcal{J}_{\text{platoon}}(s)\|_\infty \leq 1 \& \quad j(t) > 0 \quad (12)$$

We remark that we adopt \mathcal{L}_∞ norms of the string stability instead of \mathcal{L}_2 norms. Although \mathcal{L}_2 norms can provide clearer derivation, it only deals with the energy dissipation in the upstream direction and not the peak of perturbations (Darbha, 2003). In addition, the head-to-tail string stability, also named weakly single final string stability, is adopted in this paper for string stability analyses since it can deal with the relationship between peaks of perturbation before and after it spread over the platoon. So that the string stability indicates the perturbation is not amplified by the CACC platoon (Stüdli et al., 2017).

3.2. Controller switching method: Youla-Kucera parametrization

Although the controllers are designed to maintain string stability of platoon under different platoon size, the switching of the controller will cause perturbations inevitably, which will cause safety hazards in the traffic flow. Therefore, a parameterization method for smooth switching between different controllers is needed to ensure the feasibility of the above CACC controller design.

Youla-Kucera (YK) parametrization is a method to stabilize the class of a given plant that contains all stabilizing controllers (Dasgupta and Anderson, 1996; Navas et al., 2017). One of the advantages of this method is that the performance transfer function is tuned with a special parameter, which means that the stability of unstable open-loop controllers can be maintained while switching between controllers.

3.2.1. Fundamentals on YK parametrization

The basis of YK parametrization is described in detail below, which includes doubly coprime factorization and YK parameterization of all stabilizing controllers.

Basic notations are introduced below. $\mathbb{R}H_\infty$ is the real stable transfer function space; G and K_i maintain the same definitions as in Section 3.

For applying YK parametrization, internal dynamics of the vehicles G need to be presented as state-space representation:

$$\begin{aligned}\dot{m}(t) &= Am(t) + Bu(t), \\ x(t) &= Cm(t) + Du(t),\end{aligned} G(s) = \begin{bmatrix} A & B \\ C & D \end{bmatrix}, \quad (13)$$

where t indicates time, $m(t)$ is the state vector, $\dot{m}(t)$ is the evolution of the state vector over time, $x(t)$ is the output vector, and $u(t)$ is the control vector. A, B, C, D are the constant coefficients matrices of state-space matrices of G .

Any appropriate controller K_i could stabilize this system, which is represented as:

$$\begin{aligned}\dot{n}(t) &= A_i^c n(t) + B_i^c e(t), \\ u(t) &= C_i^c n(t) + D_i^c e(t),\end{aligned} K_i(s) = \begin{bmatrix} A_i^c & B_i^c \\ C_i^c & D_i^c \end{bmatrix}, \quad (14)$$

where $n(t)$ is the state vector, and A_i^c, B_i^c, C_i^c and D_i^c are the constant coefficients matrices of state-space matrices of K_i . It should be noted that K_0 represents the initial controller and K_1 represents the controller after a complete switch, thanks to YK parametrization.

3.2.2. Doubly coprime factorization

Factorization means the plant and controllers are represented as the products of two transfer functions. coprimeness refers to absence of common zeros in the right half-plane, and double coprimeness excludes unstable pole/zero cancellations, and refers to the idea of being right and left coprime.

The coprime factors of G and K_i can be expressed as:

$$G = NM^{-1} = \tilde{M}^{-1}\tilde{N}, K_i = U_i V_i^{-1} = \tilde{V}_i^{-1}\tilde{U}_i, \quad (15)$$

where coprime factors $N, M, \tilde{M}, \tilde{N}, U_i, V_i, \tilde{U}_i, \tilde{V}_i \in \mathbb{R}H_\infty$ satisfy double Bezout's identity (Pommaret and Quadrat, 1998):

$$\begin{bmatrix} \tilde{V}_i & -\tilde{U}_i \\ -\tilde{N} & \tilde{M} \end{bmatrix} \begin{bmatrix} M & U_i \\ N & V_i \end{bmatrix} = \begin{bmatrix} M & U_i \\ N & V_i \end{bmatrix} \begin{bmatrix} \tilde{V}_i & -\tilde{U}_i \\ -\tilde{N} & \tilde{M} \end{bmatrix} = \begin{bmatrix} I & 0 \\ 0 & I \end{bmatrix}. \quad (16)$$

Using the relationship of state-space representation and transfer function $G(s) = C(sI - A)^{-1}B$ and $K_i(s) = C_i^c(sI - A_i^c)^{-1}B_i^c + D_i^c$, coprime factors can be derived by:

$$\begin{bmatrix} M & U_i \\ N & V_i \end{bmatrix} = \left[\begin{array}{cc|cc} A + BF & 0 & -B & 0 \\ 0 & A_i^c + B_i^c F_i^c & 0 & B_i^c \\ \hline -F & C_i^c + D_i^c F_i^c & I & D_i^c \\ -C & F_i^c & 0 & I \end{array} \right], \quad (17)$$

$$\begin{bmatrix} \tilde{V}_i & -\tilde{U}_i \\ -\tilde{N} & \tilde{M} \end{bmatrix} = \left[\begin{array}{cc|cc} A + BD_i^c C & BC_i^c & -B & BD_i^c \\ B_i^c C & A_i^c & 0 & B_i^c \\ \hline F_i - D_i^c C & -C_i^c & I & -D_i^c \\ C & -F_i^c & 0 & I \end{array} \right], \quad (18)$$

where F and F_i^c should be chosen such that $A + BF, A_i^c + B_i^c F_i^c \in \mathbb{R}H_\infty$. Straight lines indicate the elements of the matrix that belong to each factor, respectively. The proof of the Equation (17-18) detailed in Appendix B.

During the process of controller switching, only the vehicle decision controller K_i from K_0 switches to K_1 and internal dynamics of the vehicles G remain unchanged, which means M and N remain unchanged while U_0, V_0 are converted to U_1, V_1 .

3.2.3. YK parameterization of all stabilizing controllers

The fundamental of YK parametrization is the initial interpolation controller with a parameter Q to obtain all controllers K that can stabilize a given plant G . The expression of $K(Q)$ and Q is described as:

$$K(Q) = (U_0 + M\gamma Q)(V_0 + N\gamma Q)^{-1} = (\tilde{V}_0 + \gamma Q\tilde{N})^{-1}(\tilde{U}_0 + \gamma Q\tilde{M}), Q \in \mathbb{R}H_\infty^{pxm}, \quad (19)$$

$$Q = \tilde{U}_1 - \tilde{V}_1\tilde{V}_0^{-1}\tilde{U}_0, \quad (20)$$

where $\gamma \in [0, 1]$ is a scalar factor playing a pivotal role as a switching signal in controller interpolation, indicating the level of interconnection of the two controllers (Niemann and Stoustrup, 1999). When $\gamma = 0$, the controller is completely taken over by K_0 , while K_1 is fully controlled when $\gamma = 1$.

Proof: First check the matrix of closed-loop feedback control system.

$$\begin{aligned} \begin{bmatrix} I & -K(Q) \\ -G & I \end{bmatrix}^{-1} &= \begin{bmatrix} I & -(\tilde{V}_0 + \gamma Q\tilde{N})^{-1}(\tilde{U}_0 + \gamma Q\tilde{M}) \\ -\tilde{M}^{-1}\tilde{N} & I \end{bmatrix}^{-1} \\ &= \left\{ \begin{bmatrix} (\tilde{V}_0 + \gamma Q\tilde{N})^{-1} & 0 \\ 0 & \tilde{M}^{-1} \end{bmatrix} \begin{bmatrix} \tilde{V}_0 + \gamma Q\tilde{N} & -(\tilde{U}_0 + \gamma Q\tilde{M}) \\ -\tilde{N} & \tilde{M} \end{bmatrix} \right\}^{-1} \\ &= \begin{bmatrix} M & U_0 + M\gamma Q \\ N & V_0 + N\gamma Q \end{bmatrix} \begin{bmatrix} \tilde{V}_0 + \gamma Q\tilde{N} & 0 \\ 0 & \tilde{M} \end{bmatrix} \\ &= \left\{ \begin{bmatrix} M & U \\ N & V \end{bmatrix} + \begin{bmatrix} 0 & MQ \\ 0 & NQ \end{bmatrix} \right\} \left\{ \begin{bmatrix} \tilde{V} & 0 \\ 0 & \tilde{M} \end{bmatrix} + \begin{bmatrix} Q\tilde{N} & 0 \\ 0 & 0 \end{bmatrix} \right\} \\ &= \begin{bmatrix} M & U \\ N & V \end{bmatrix} \begin{bmatrix} \tilde{V} & 0 \\ 0 & \tilde{M} \end{bmatrix} + \begin{bmatrix} MQ\tilde{N} & 0 \\ NQ\tilde{N} & 0 \end{bmatrix} + \begin{bmatrix} 0 & MQ\tilde{M} \\ 0 & NQ\tilde{M} \end{bmatrix} \\ &= \begin{bmatrix} \tilde{V} & -\tilde{U} \\ -\tilde{N} & \tilde{M} \end{bmatrix}^{-1} \begin{bmatrix} \tilde{V}^{-1} & 0 \\ 0 & \tilde{M}^{-1} \end{bmatrix}^{-1} + \begin{bmatrix} MQ\tilde{N} & MQ\tilde{M} \\ NQ\tilde{N} & NQ\tilde{M} \end{bmatrix} \\ &= \begin{bmatrix} M & U \\ N & V \end{bmatrix} \begin{bmatrix} \tilde{V} & 0 \\ 0 & \tilde{M} \end{bmatrix} + \begin{bmatrix} M \\ N \end{bmatrix} Q \begin{bmatrix} \tilde{N} & \tilde{M} \end{bmatrix} \\ &= \begin{bmatrix} I & -K \\ -G & I \end{bmatrix}^{-1} + \begin{bmatrix} M \\ N \end{bmatrix} Q \begin{bmatrix} \tilde{N} & \tilde{M} \end{bmatrix} \in \mathbb{R}H_\infty^{pxm}. \end{aligned} \quad (21)$$

From Equation (21), it is clearly that any controller $K(Q)$ parameterized by $Q \in \mathbb{R}H_\infty^{pxm}$ stabilizes the plant G according to the Corollary 4.2 in references (Tay et al., 1998; Mahtout et al., 2020).

The closed-loop poles of the system during the switching process are the combination of $[G, K_0]$ and $[G, K_1]$, which can maintain the stability of the system under any combination of Q and γ , thus ensuring the stable switch of the controllers independent of γ (Niemann and Stoustrup, 1999).

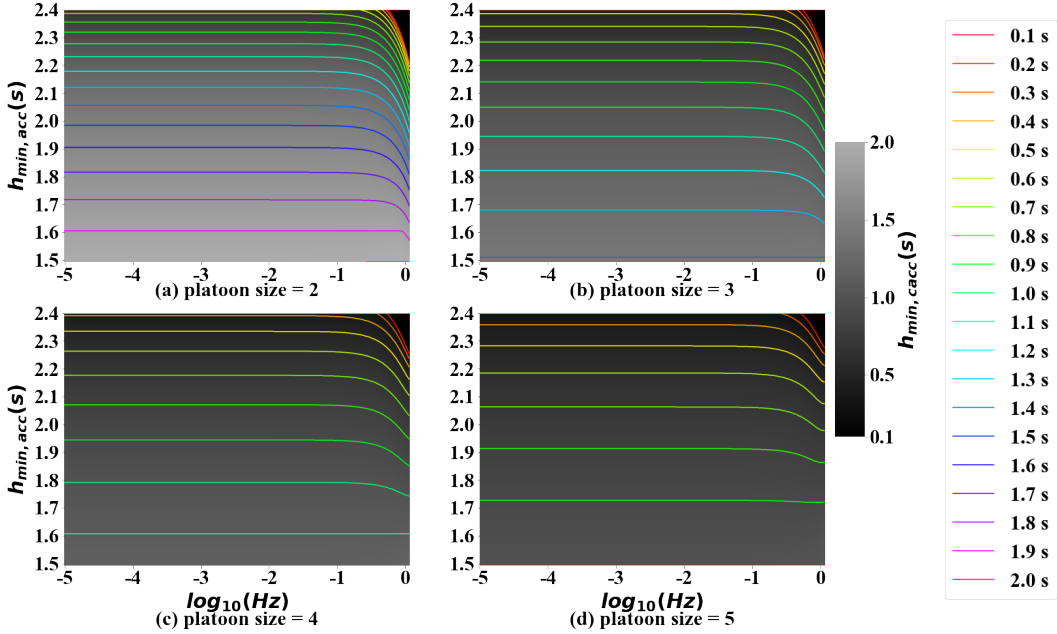
4. Theoretical analyses

In this section, the detailed controller design process is carried out using the methodology proposed in Section 3. The process includes selecting the best desired time gap strategy for ACC and CACC in the case of CACC platoon, determining YK parameter in the controller switching of ACC and CACC, and deciding γ function. In addition, to facilitate subsequent calculations and experiments, the above-defined controller coefficients selected in this paper are as follows which is set based on existing researches (Milanés and Shladover, 2014; Milanés et al., 2013; Navas et al., 2016) and field experiments employed detailed in Appendix A. Moreover, the maximum platoon size S of CACC platoon is set to 5 in the paper which is absolutely feasible and effective for communication latency and packet loss rates in the perspective of the communication technology.

Table 1

Parameters chosen for ACC and CACC controller.

Parameter	k_p	k_d	τ_i	k_G	ϕ_i	θ_i
Value	0.45 s^{-2}	0.25 s^{-1}	0.7862 s/rad	0.9403	0.2 s.	0.3 s

**Figure 4:** Contour plot of perturbation frequency versus $h_{min,acc}$, indicating the corresponding minimal value for $h_{min,cacc}$.

4.1. Analyses of string stability

When the CACC platoon is formed, taking the CACC platoon as the control object can maintain a smaller desired time gap without losing string stability. In order to explore the minimum desired time gap combination for the CACC platoon, the theoretical analyses regarding string stability are carried out using the method proposed in Section 3.1.

As for the desired time gap $h_i = h_{i,min}$, margin string stability criterion (12) is met, and string stability can be guaranteed when $h_i \geq h_{i,min}$ (Naus et al., 2010). However, due to the complexity of the CACPC structure, the calculation of the minimum desired time gap $h_{i,min}$ is too complicated and cannot give an algebraic equation of h_{acc} and h_{cacc} , so the derivation is not discussed here. A numerical approximation approach is adopted to explore the combination of $h_{min,acc}$ and $h_{min,cacc}$ as margin string stable. Moreover, since the perturbation faced in real traffic conditions is considered to be of infinite wavelength (Bian et al., 2019; Xiao and Gao, 2011), we only focus on the magnitude of the transfer function under low frequency ($10^{-5} - 10^0$ Hz) (Onca et al., 2014). Fig. 4 shows that $h_{min,cacc}$ changes with $h_{min,acc}$ over different frequencies where colored contour lines in Fig. 4 represent the stability demarcation lines of the combination of $h_{min,acc}$ and $h_{min,cacc}$. Furthermore, the heatmap shows the margin stable $h_{min,cacc}$ under different $h_{min,acc}$ and perturbation frequency.

It can be clearly found in Fig. 4, CACC can maintain a smaller desired time gap with platoon size increasing. Moreover, $h_{min,cacc}$ can significantly decrease with $h_{min,acc}$ increasing, which means the feasibility of eliminating the redundancy within the CACC platoon through the appropriate deployment of the desired time gap. In addition, string stability can be significantly improved as the frequency of perturbation approaches 10^0 Hz, which is represented as the arc under $10^{-0.5} - 10^0$ Hz in Figure 4. When we focus on the region of $10^{-5} - 10^{-0.5}$ Hz, an interesting phenomenon is discovered that $h_{min,cacc}$ stays the same as the frequency increases, which means the combination of $h_{min,cacc}$ and $h_{min,acc}$ to guarantee the string stability is determined for a specific platoon size.

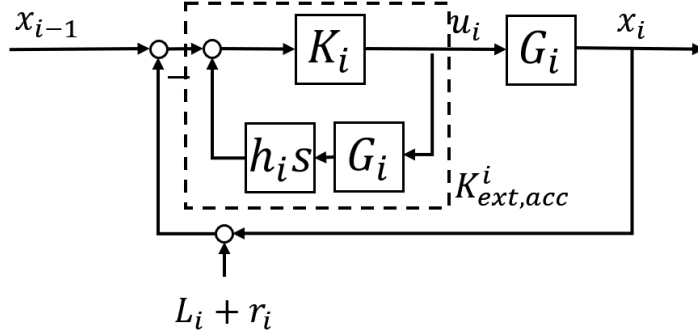


Figure 5: Equivalent ACC control structure.

Based on the conclusions obtained above, in order to maximize the capacity while ensuring string stability and safety, we choose $h_{1,acc} = 2s$ and $h_{1,cacc} = 0.4s$ for the case of $S = 5$ while the desired time gap settings of ACC and CACC for the case of $S = 2$ are $h_{0,acc} = 2.108s$ and $h_{0,cacc} = 0.747s$ in this paper.

4.2. Analyses of controller switching

For the LV in a CACC platoon, since it cannot communicate with the predecessor vehicle, it loses the information gain from the communication module, so its control system is represented by standard ACC, as shown in Fig. 2 (a).

4.2.1. Modify ACC controller

To incorporate the desired time gap into the controller, the ACC controller in Fig. 2 (a) is reconstructed so that the ACC controller can perform stable interpolation for the different desired time gap h_i . And the corresponding equivalent ACC control structure is shown in Fig. 5. The transfer function of the extended controller is as follows:

$$K_{ext,acc}^i(s) = \frac{K_i}{1 + h_i G_i K_i s}. \quad (22)$$

4.2.2. YK parametrization for ACC controller

Based on the mathematical basis introduced in Section 3.2, the control structure applied to controller switching needs to be modified accordingly by introducing a dual coprime factor. The control structure for switching based on left coprime factors is shown in Fig. 6:

For stable switching purposes, coprime factors need to meet double Bezout's identity as shown in Equation (16) based on the state-space matrix of transfer functions of $K_{0,acc}, K_{1,acc}$. The specific transfer functions of coprime factors are as follows:

$$\begin{aligned} U_0 &= \frac{-s(s + 1.272)(s + 1.8)}{(s + 4.42)(s^2 + 1.836s + 1.027)}, \\ V_0 &= \frac{-4(s^2 + 1.902s + 1.135)}{(s + 4.42)(s^2 + 1.836s + 1.027)}, \\ U_1 &= \frac{-s(s + 1.272)(s + 1.8)}{(s + 4.42)(s^2 + 1.808s + 0.9741)}, \\ V_1 &= \frac{-4(s^2 + 1.87s + 1.076)}{(s + 4.42)(s^2 + 1.808s + 0.9741)}. \end{aligned} \quad (23)$$

As for the YK parameter Q_{acc} , substitute coprime factors into Equation(20):

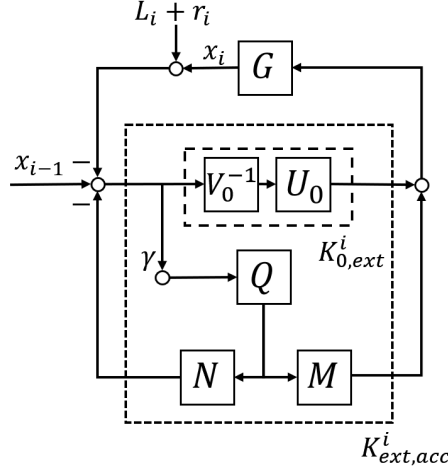


Figure 6: YK control structure for ACC controllers switching.

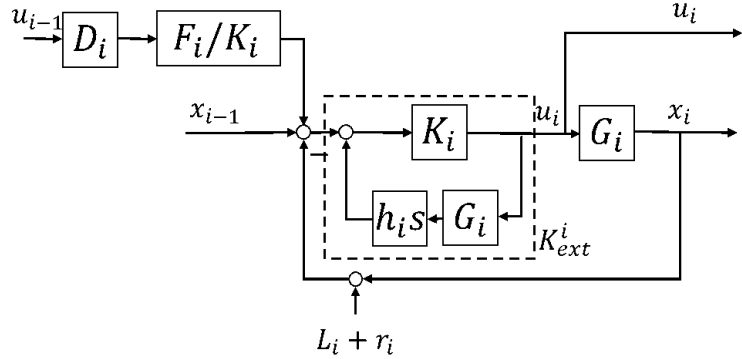


Figure 7: Equivalent CACC control structure.

$$Q_{acc} = \frac{-0.1005(s + 1.892)(s + 4.38)(s + 4.42) (s^2 + 1.82s + 0.9968) (s^2 + 1.969s + 1.238)}{(s + 4.42)^3 (s^2 + 1.808s + 0.9741) (s^2 + 1.836s + 1.027)^2}. \quad (24)$$

4.2.3. Modify CACC controller

Similar to the method adopted in Section 4.2.1, the system construction drawing of the CACC controller is in Figure. 3, which is reconstructed to incorporate the desired time gap h_i into the controller. And the corresponding equivalent CACC control structure is shown in Figure. 7. The transfer function of the extended controller is as follows:

$$K_{ext,cacc}^i(s) = \frac{K_i}{1 + h_i G_i K_i s}. \quad (25)$$

4.2.4. YK parametrization for CACC controller

Similar to Section 4.2.2, the control structure applied to controller switching needs to be modified accordingly by introducing a dual coprime factor based on the mathematical basis presented in Section 3.2. The control structure for switching based on left coprime factors is shown in Figure. 8:

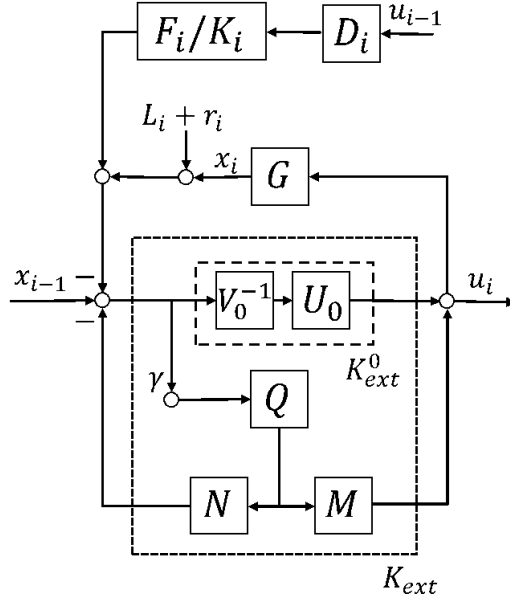


Figure 8: YK control structure for CACC controllers switching.

Based on Equation (17-18), coprime factors which meet double Bezout's identity as shown in Equation (16) can be obtained easily. The specific transfer functions of coprime factors are as follows:

$$\begin{aligned}
 U_3 &= \frac{-s(s+1.272)(s+1.8)}{(s+4.406)(s+1.159)(s+0.3148)}, \\
 V_3 &= \frac{-4(s+1.144)(s+0.3515)}{(s+4.406)(s+1.159)(s+0.3148)}, \\
 U_4 &= \frac{-s(s+1.272)(s+1.8)}{(s+4.397)(s+1.226)(s+0.1438)}, \\
 V_4 &= \frac{-4(s+1.221)(s+0.1587)}{(s+4.397)(s+1.226)(s+0.1438)}.
 \end{aligned} \tag{26}$$

As for the YK parameter Q_{cacc} , substitute coprime factors into Equation(20):

$$Q_{cacc} = \frac{-0.4451(s+4.402)(s+3.51)(s+1.918)(s+1.8)(s+1.274)(s+1.219)(s+1.414)(s+0.3596)(s+0.1572)}{(s+4.397)(s+1.8)(s+1.272)(s+1.226)(s+0.1438)(s+4.406)^2(s+0.3148)^2(s^2+2.319s+1.344)}. \tag{27}$$

4.3. Tuning function γ for CACC platoon

The theoretical results of Section 4.1 point out that different CACC platoon sizes have different combinations of $h_{min,acc}$ and $h_{min,cacc}$ as string stability margin. To avoid being restricted by the platoon size, a corresponding tuning function γ for the platoon size is required so that CACPC can be applied under different platoon sizes.

The theoretical results of Section 4.1 indicate that different CACC platoon sizes have different combinations of $h_{min,acc}$ and $h_{min,cacc}$ as string stability margin. In order to avoid being restricted by the platoon size, the corresponding tuning function γ about platoon size is required so that CACPC can be applied under different platoon sizes. Based on the reasons above, a numerical analysis is conducted to obtain the combination of γ_{acc} and γ_{cacc} which can maintain string stability of CACC platoon under different platoon sizes. The results are shown in Figure. 9, where the transparent gray plane and the curve on it represent the string stability margin plane and the intersection of the string stability margin plane and the amplitude surface. It is worth noting that Figure. 9 is carried out at the frequency of 10^{-5} Hz and further exploration that covers a broader frequency domain is carried out in Section 5.1.

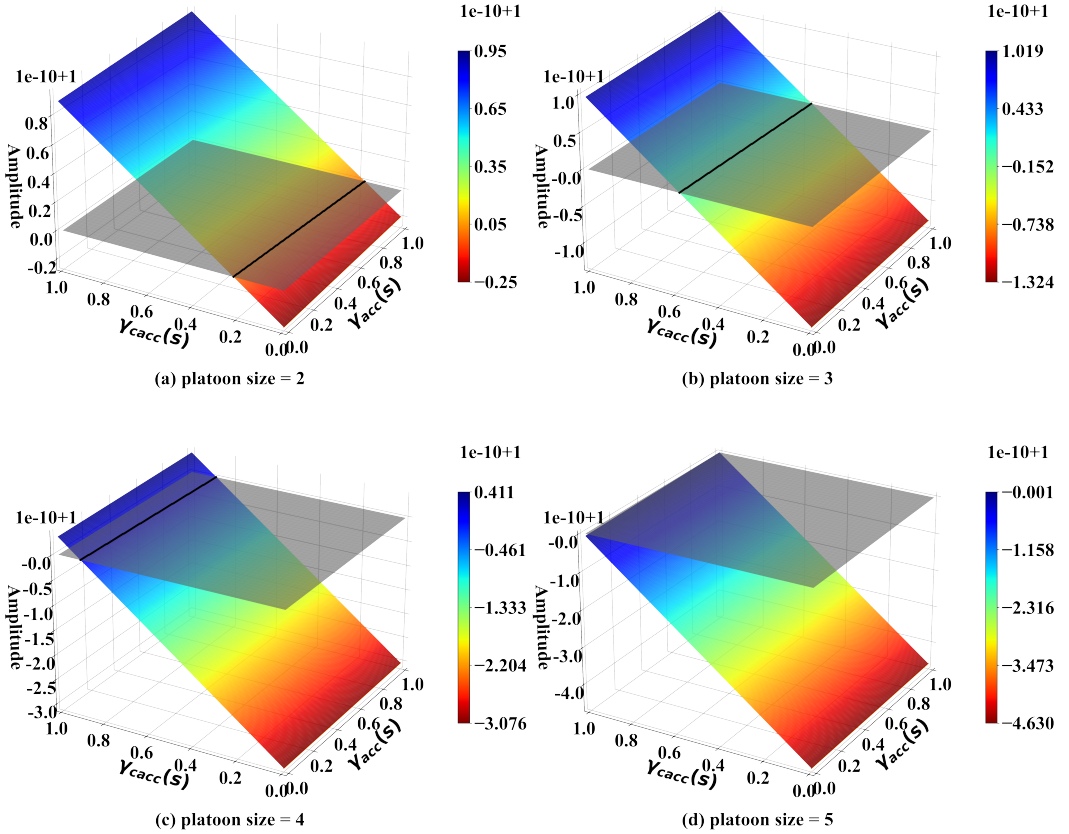


Figure 9: String stability's surface depending on YK γ_{acc} and γ_{cacc} .

We can conclude from Figure. 9 that the intersection of the transparent plane and string stability's surface is the basis for selecting γ_{acc} and γ_{cacc} , which can ensure string stability and tap the advantages of CACPC as much as possible. Through the curve-fitting method, we can get the expression of the intersection as follows (since any γ can meet the string stability at platoon size = 5, there is no corresponding expression.):

$$\gamma_{cacc} = \begin{cases} -0.0501 * \gamma_{acc} + 0.2221, & \text{if } n = 2 \\ -0.0248 * \gamma_{acc} + 0.5815, & \text{if } n = 3 \\ -0.0165 * \gamma_{acc} + 0.8995, & \text{if } n = 4 \end{cases} \quad (28)$$

Considering the gain-scheduling method, the appropriate tuning function γ is derived based on the expression above:

$$\gamma_{acc} = \begin{cases} 0, & \text{if } n = 1 \\ 0.4, & \text{if } n = 2 \\ 0.7, & \text{if } n = 3 \\ 0.9, & \text{if } n = 4 \\ 1, & \text{if } n = 5 \end{cases}, \quad (29)$$

$$\gamma_{cacc} = \begin{cases} 0, & \text{if } n = 1 \\ 0.3, & \text{if } n = 2 \\ 0.6, & \text{if } n = 3 \\ 0.9, & \text{if } n = 4 \\ 1, & \text{if } n = 5 \end{cases}, \quad (30)$$

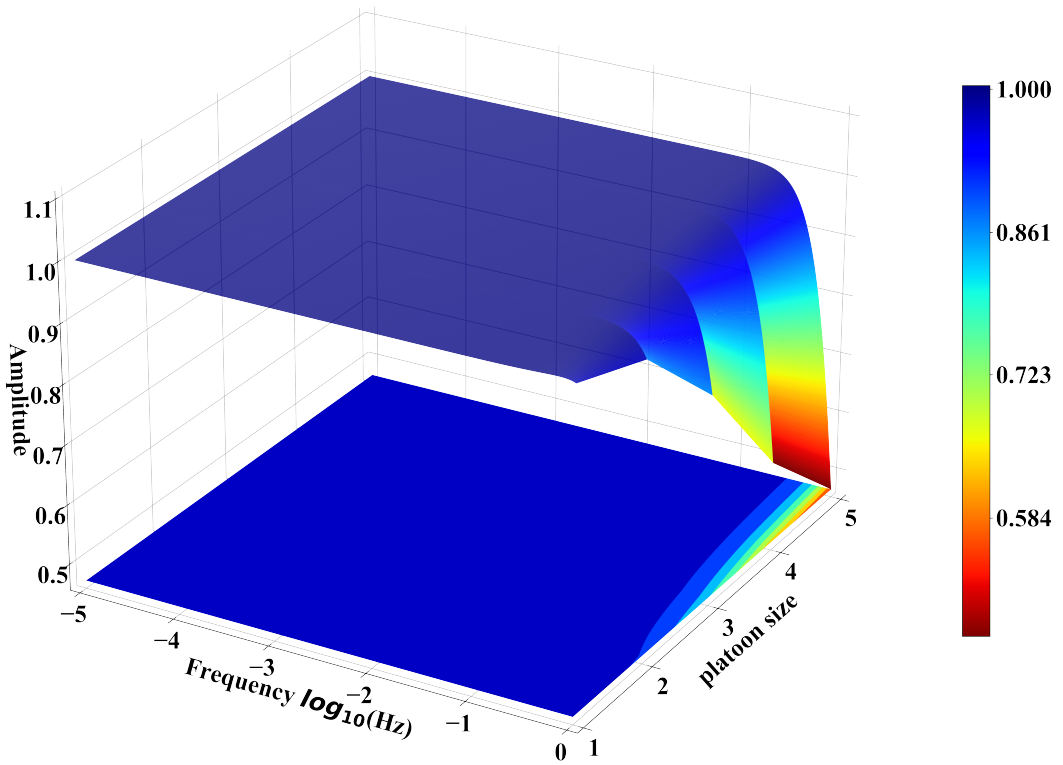


Figure 10: String stability's surface depending on platoon size.

where, n denotes platoon size.

5. Numerical analyses

In this section, we first validate the string stability of CACPC based on the theoretical result derived in Section 4 by numerical simulation. Then a series of simulation experiments are conducted to explore the impact of YK parameterization on dynamic performance.

5.1. Validation of string stability

Based on the results in Section 4.2 and 4.3, we have obtained the amplitude of CACPC under different platoon sizes. It is necessary to keep the string stable to prevent the perturbation from being amplified during propagation. Therefore, a numerical experiment is conducted to explore the string stability of CACC platoon under low frequency ($10^{-5} - 10^0$ Hz). Figure. 10 shows the result where the curved surface represents the amplitude of the CACC platoon under low frequency ($10^{-5} - 10^0$ Hz) and different platoon sizes.

Figure. 10 indicates that the CACPC proposed above can avoid amplifying perturbation which means it can maintain string stability during the switching process.

5.2. Simulation experiments of YK parameterization

Behaviors observed in simulation experiments are closer to those in the real traffic environment compared to theoretical analyses. In order to further explore the actual effect of the controller switching using the YK

parameterization, a series of simulation experiments are carried out based on CACPC as a supplement to the theoretical analysis.

5.2.1. Simulation experiments maintain a constant speed during the forming and splitting process

Simulation scenario: The simulation scenario is set as: at first, a leader vehicle drives on an infinitely long road under a given speed and acceleration configuration(containing five same small perturbations that occurred at the simulation time of 300s, 1000s, 1700s, 2400s, and 3100s under different platoon size). There are four experiments conducted:

1. *Experiment one:* The forming process of the CACC platoon with YK parameterization where an ACC (which is a CACC but degraded to an ACC functionally) follows the leader at the beginning, and more CACCs join the CACC platoon one by one at the simulation time of 700s, 1400s, 2100s, and 2800s.
2. *Experiment two:* The forming process of the CACC platoon without YK parameterization where an ACC (which is a CACC but degraded to an ACC functionally) follows the leader at the beginning, and more CACCs join the CACC platoon one by one at the simulation time of 700s, 1400s, 2100s, and 2800s.
3. *Experiment three:* The splitting process of the CACC platoon with YK parameterization where an ACC (which is a CACC but degraded to an ACC functionally) follows the leader at the beginning, and more CACCs join the CACC platoon one by one at the simulation time of 700s, 1400s, 2100s, and 2800s.
4. *Experiment four:* The splitting process of the CACC platoon without YK parameterization where an ACC (which is a CACC but degraded to an ACC functionally) and four CACCs follow the leader at the beginning, and the last CACC in the platoon leaves one by one at the simulation time of 700s, 1400s, 2100s, and 2800s.

The first pair of experiments is the forming process of the CACC platoon where an ACC (which is a CACC but degraded to an ACC functionally) follows the leader at the beginning, and more CACCs join the CACC platoon one by one at the simulation time of 700s, 1400s, 2100s, and 2800s. Moreover, periodic perturbations are applied to the leader to explore the string stability of the CACC platoon under different platoon size. Another pair of experiments are conducted simulating the splitting process of the CACC platoon. It should be noted that there are total four experiments conducted to analyze the impact of the YK parameterization under the platoon forming case and the platoon splitting case. Experiment one and three applies YK parameterization with tuning function γ proposed above, while experiment two and four switches to CACPC mode directly only the platoon size reaches maximum platoon size $S = 5$. Furthermore,

Simulation results. Figure. 11 and 13 show the results of experiments one,two, three and four, respectively. And figure. 12 and 14 show the detailed perturbation simulation results of of experiments one,two, three and four. In figure. 11 and 13, (a)-(c) show the simulation results of the case with YK parameterization and (d)-(f) show the simulation results of the case without YK parameterization where (a),(d) Acceleration of simulation results; (b),(e) Velocity of simulation results; (c),(f) Time gap of simulation results. As for figure. 12 and 14, (a)-(e) show the propagating processes of five applied perturbations and (f)-(i) show the four switching processes of the case with YK parameterization. And for the case without YK parameterization (j)-(n) show the propagating processes of five applied perturbations and (o)-(r) show the four switching processes.

In figure. 11 and 12, the process of the gradual formation of the CACC platoon with and without YK parameterization is clearly shown while the process of the gradual splitting is shown in figure. 13 and 14. The first attention is spontaneous perturbations during controller switching. From the comparison of figure. 12 and 14, we can find that the controller switching causes spontaneous perturbations in the process of platoon formation which caused by the changing of equivalent desired time gap. These spontaneous perturbations can be suppressed by applying the tuning function γ to achieve smooth switching. However, in the case without YK parameterization, due to the direct switching when the platoon size reaches or leaves the trigger size, the spontaneous perturbation is too significant, which seriously impacts the stability and safety of the traffic flow. The second attention is string stability. All CACPCs applied under different CACC platoon sizes can maintain string stability through YK parameterization which is shown in figure. 12 and 14. Moreover, using YK parameterization can work under any CACC MPR since it can be applied even in a common scenario where the CACC MPR is low and the platoon size is small. But for the case without YK parameterization, the CACPCs do not function sufficiently until the set trigger platoon size is reached which means the it is hard to function in a long period of time because there will be a long time until the CACC MPR gets high. In addition, because the splitting process and forming process is similar, the following simulation experiments are only conducted in the forming process. Notice that from the difference on the acceleration between subplot (a) and (b) in figure. 11 and 13 which is detailed shown in subplot (k-r) in figure. 12 and 14, and a misunderstood conclusion

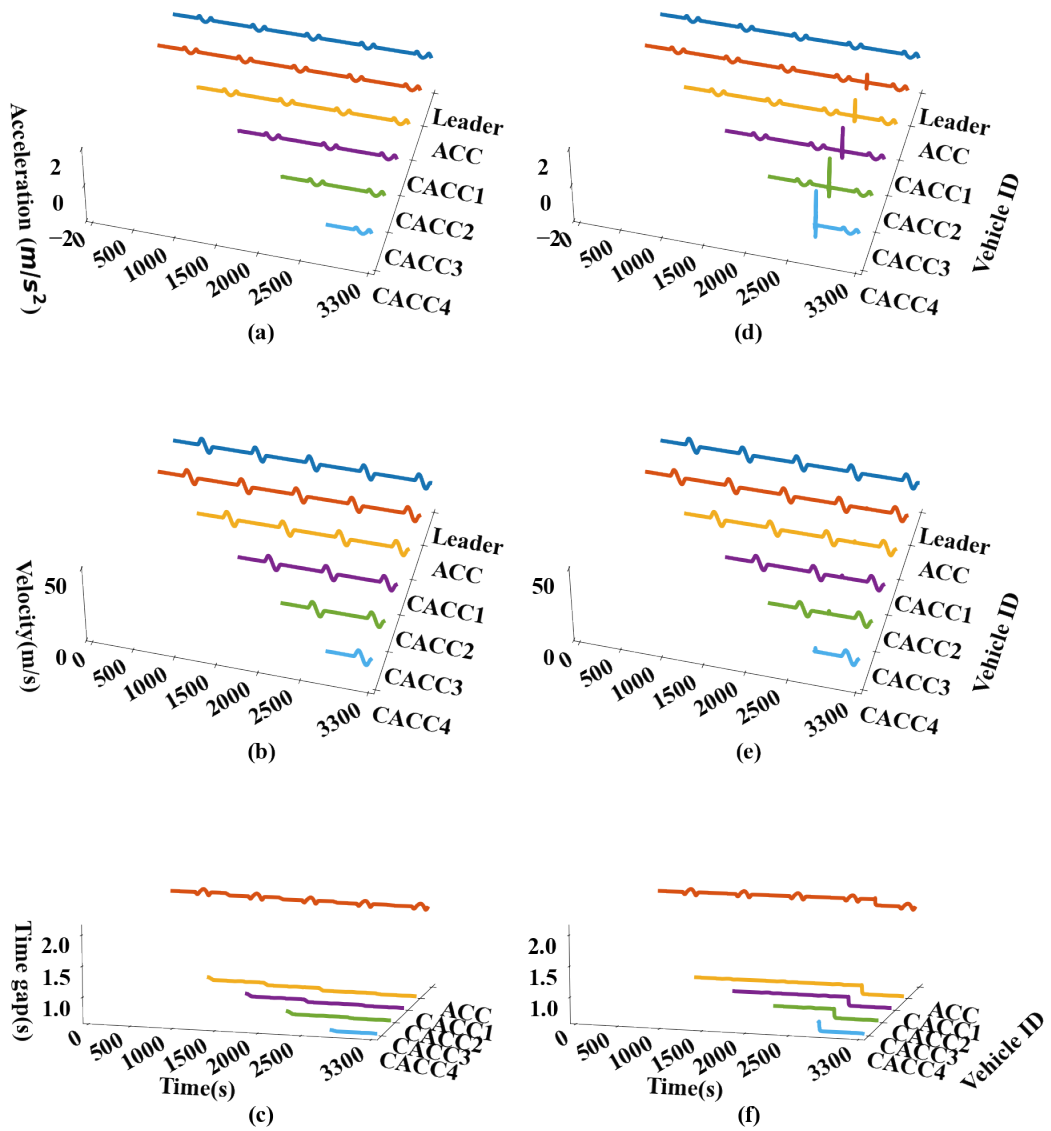


Figure 11: Simulation results of experiment one and two: CACPC with or without YK parameterization under the platoon forming case. (a)-(c) show the simulation results of experiment one and (d)-(f) show the simulation results of experiment two. (a),(d) Acceleration of simulation results; (b),(e) Velocity of simulation results; (c),(f) Time gap of simulation results.

can be drawn because the perturbation is amplified with or without YK parameterization. However, the perturbation is caused by the increasing of the equivalent desired time gap during the controller switching. In the case with YK parameterization, the perturbation only raise once then back to the equivalent state. And for the case without YK parameterization, the perturbation is fluctuating during the propagating process which means the switching progress is not smooth enough to make the perturbation suppressed.

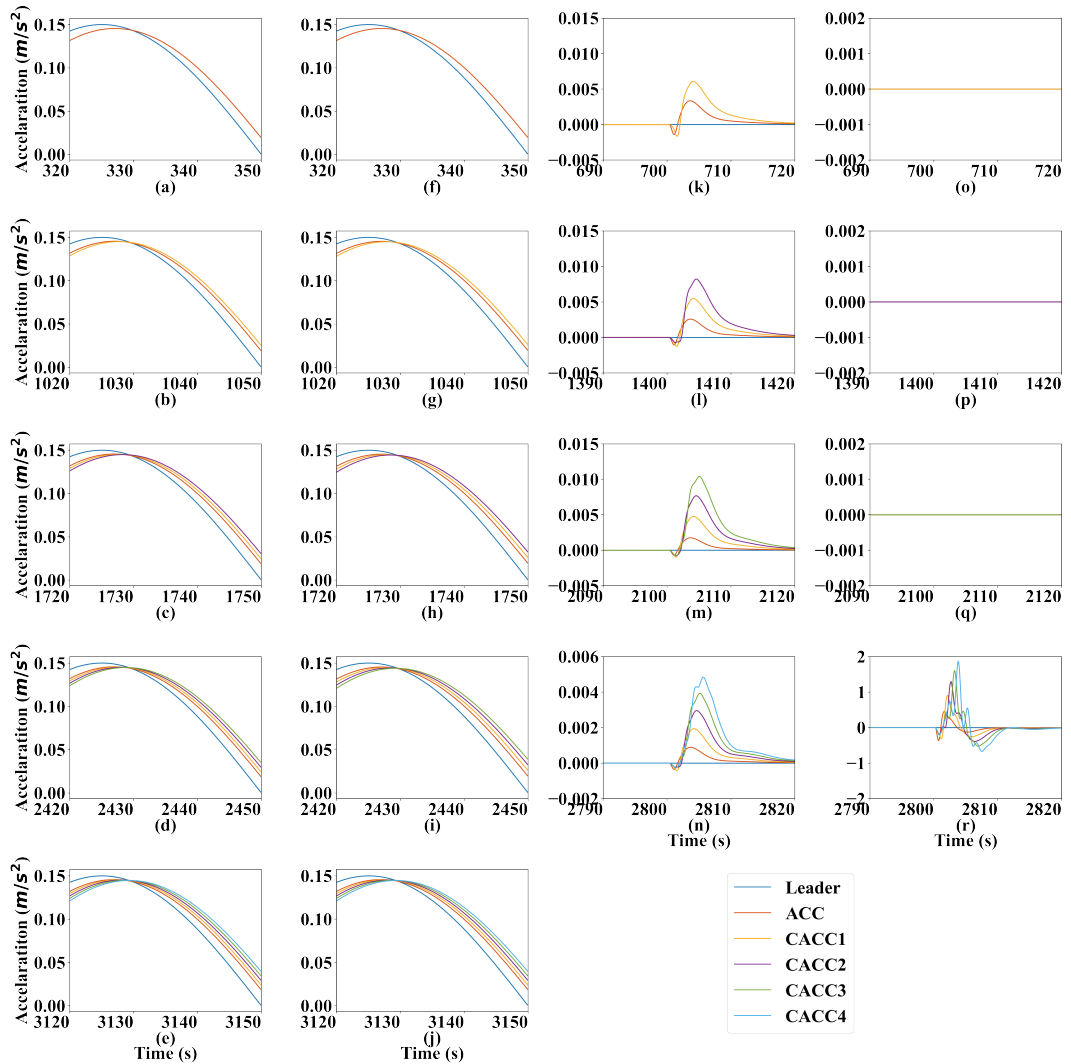


Figure 12: Detailed perturbation simulation results of experiment one and two: CACPC with or without YK parameterization under the platoon forming case. For experiment one, (a)-(e) show the propagating processes of five applied perturbations and (k)-(n) show the four switching processes. For experiment two, (f)-(j) show the propagating processes of five applied perturbations and (o)-(r) show the four switching processes.

5.2.2. Simulation experiments maintain a fluctuating speed during the forming process

Simulation scenario: The simulation scenario is similar to the experiment one in Section. 5.2.1, but different in the given speed and acceleration configuration of the leader vehicle. In this simulation experiment, the speed of leader vehicle is fluctuating all the time to simulate the traffic oscillation scenario. There are two experiments conducted:

1. *Experiment five:* The forming process of the CACC platoon with YK parameterization under the fluctuating velocity case where an ACC (which is a CACC but degraded to an ACC functionally) follows the leader at the beginning, and more CACCs join the CACC platoon one by one at the simulation time of 700s, 1400s, 2100s, and 2800s.
2. *Experiment six:* The forming process of the CACC platoon without YK parameterization under the fluctuating velocity case where an ACC (which is a CACC but degraded to an ACC functionally) follows the leader at the beginning, and more CACCs join the CACC platoon one by one at the simulation time of 700s, 1400s, 2100s, and 2800s.

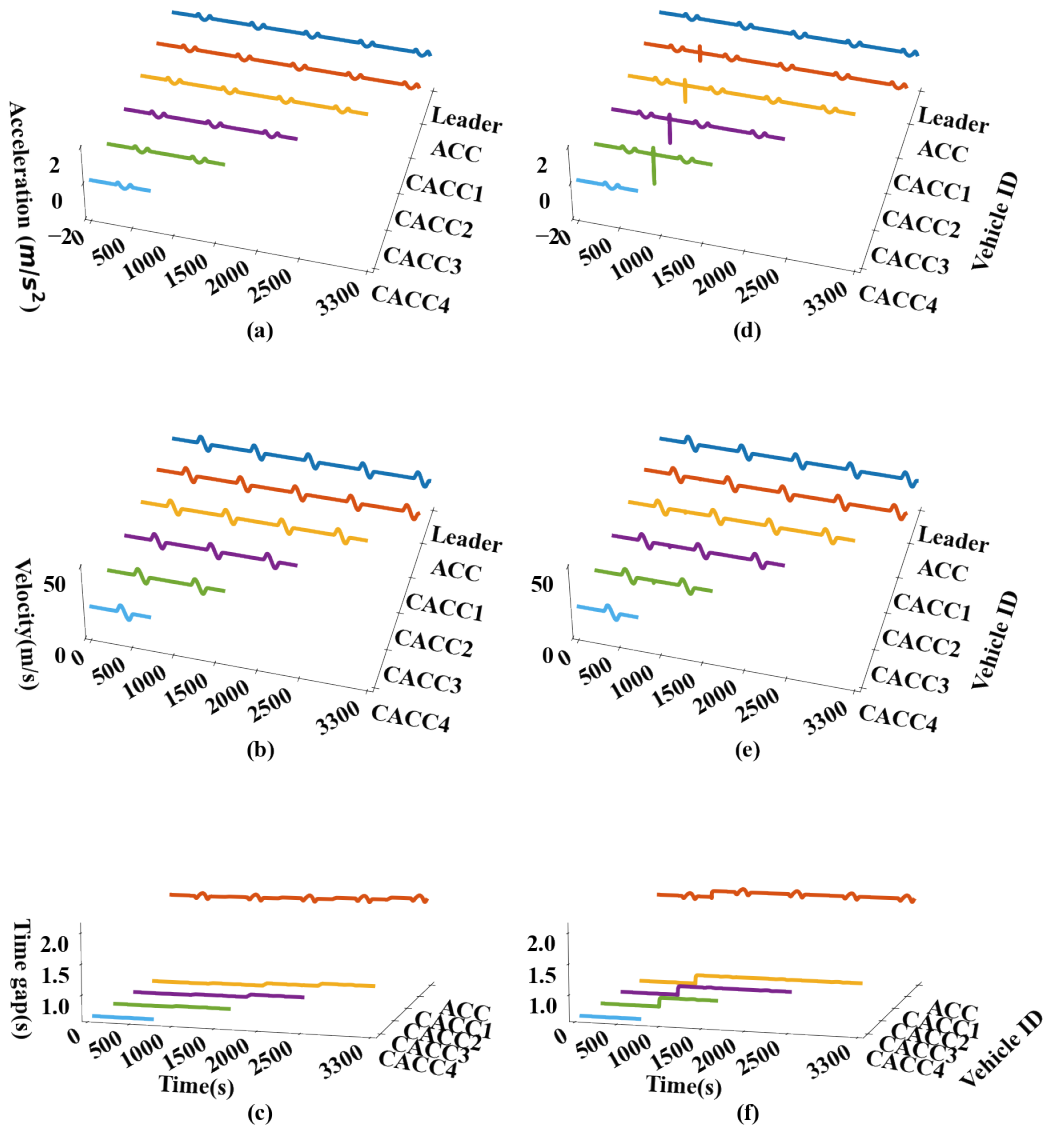


Figure 13: Simulation results of experiment three and four: CACPC with or without YK parameterization under the platoon splitting case. (a)-(c) show the simulation results of experiment three and (d)-(f) show the simulation results of experiment four. (a),(d) Acceleration of simulation results; (b),(e) Velocity of simulation results; (c),(f) Time gap of simulation results.

Simulation results. Figure. 15, 16 show the results of experiments five and six from global and local perspective respectively. The format of figure. 15, 16 is same as figure. 11, 12. For the sake of simplicity, the detailed introduction is omitted. In Figure. 15, the top graph plots the vehicles' accelerations, the median graph plots the vehicles' velocities during the simulation, and the bottom graph plots the time gap during the simulation in each figure.

From the figure. 15, the simulation results under the traffic oscillation scenario are similar to the results with constant velocity. The corresponding detailed simulation results are shown in figure. 16. The spontaneous perturbations caused by the controller switching are not significant which have the magnitude of 0.015 m/s^2 with the YK

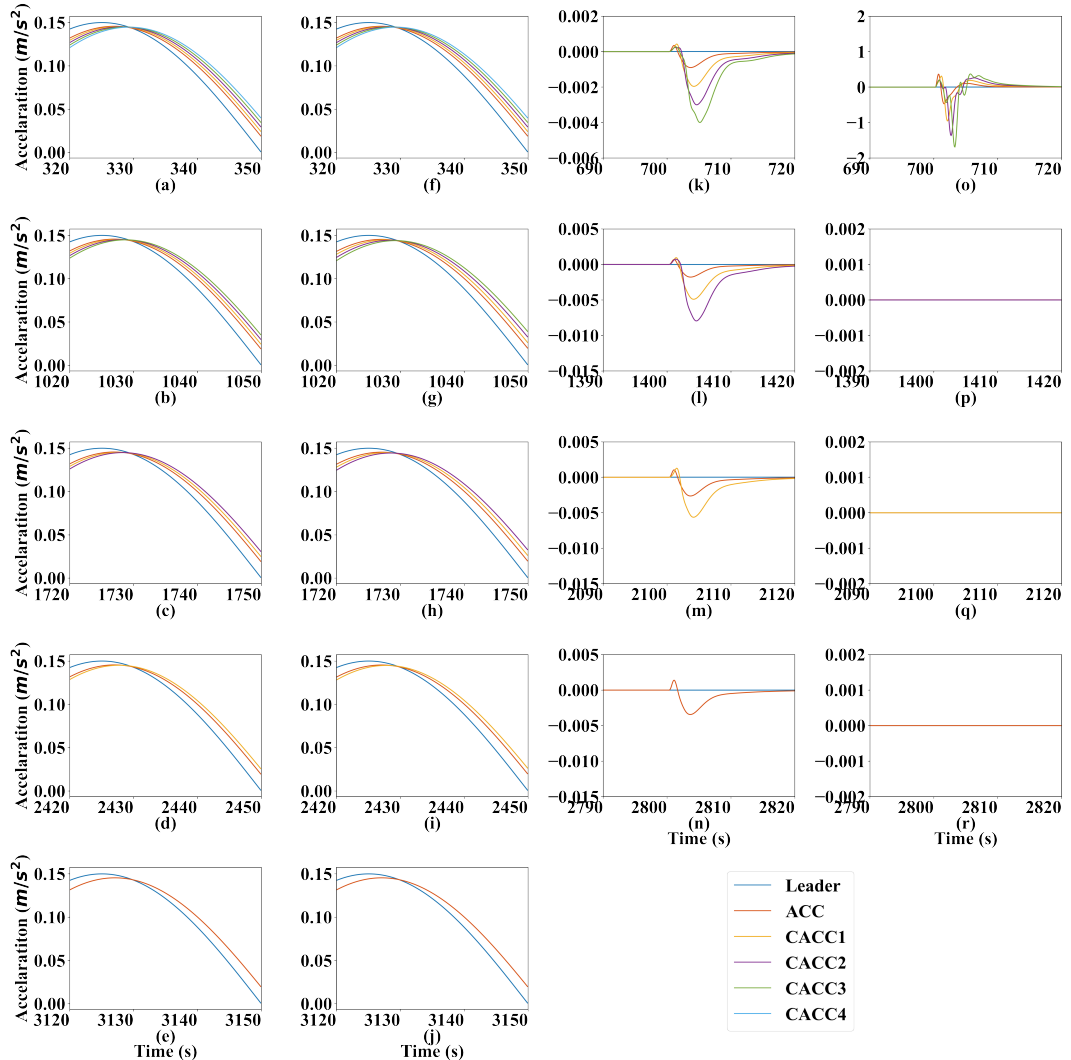


Figure 14: Detailed perturbation simulation results of experiment three and four: CACPC with or without YK parameterization under the platoon splitting case. For experiment three, (a)-(e) show the propagating processes of five applied perturbations and (k)-(n) show the four switching processes. For experiment four, (f)-(j) show the propagating processes of five applied perturbations and (o)-(r) show the four switching processes.

parameterization while the perturbation have the magnitude of $2.15m/s^2$ for the case without YK parameterization under the traffic oscillation scenario. And a noticeable rise appears in the speed graph which means a significant negative impact on traffic safety. A conclusion can be drawn that the YK parameterization can ensure the smooth switching of the controllers whether it is traffic oscillation or equilibrium state.

5.2.3. Simulation experiments maintain a constant speed during the multiple CACCs forming process

Simulation scenario: The simulation scenario of experiment seven is set as: at first, a leader vehicle drives on an infinitely long road under a given speed and acceleration configuration which is similar to the experiment one in Section. 5.2.1. There is only three perturbations at the simulation time of 300s, 1000s and 1700s. And the forming process of the CACC platoon is that two CACCs join in the ACC platoon at the same time, and the forming process repeat twice at the simulation time of 700s and 1400s. Notice that only the case with YK parameterization is applied is simulated here because simulation results of the case without YK parameterization is similar to the experiment two in Section. 5.2.1.

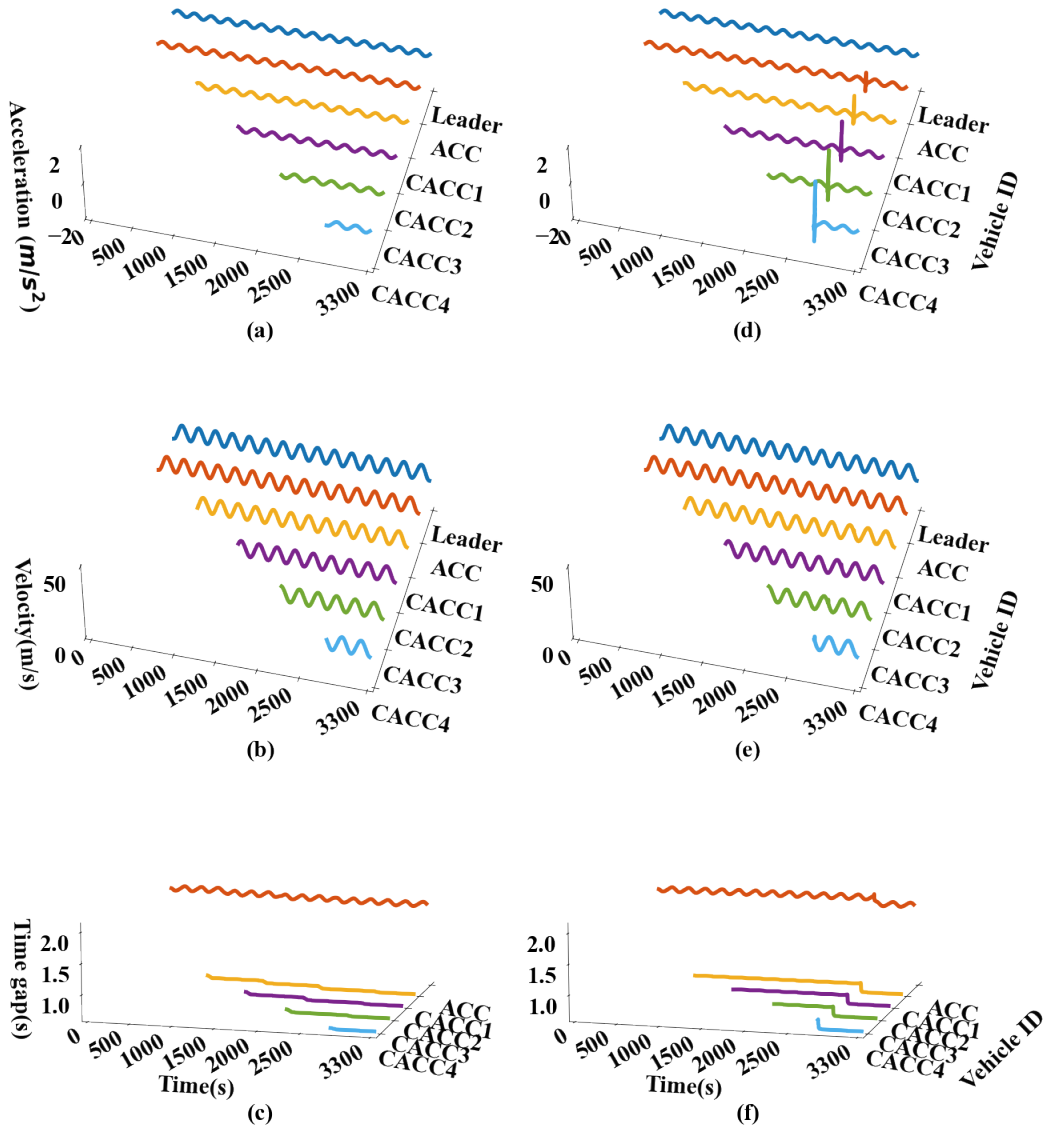


Figure 15: Simulation results of experiment five and six: CACPC with or without YK parameterization under the fluctuating velocity case. (a)-(c) show the simulation results of experiment five and (d)-(f) show the simulation results of experiment six. (a),(d) Acceleration of simulation results; (b),(e) Velocity of simulation results; (c),(f) Time gap of simulation results.

Simulation results. Figure 17 shows the results of experiments seven. In the left subplot, the top graph plots the vehicles' accelerations, the median graph plots the vehicles' velocities during the simulation, and the bottom graph plots the time gap during the simulation. And the right subplot show the detailed acceleration in 690-720s and 1390-1420s to explore the spontaneous perturbation during controllers switching.

From figure 17, the first conclusion can be drawn that YK parameterization can keep string stability even during the multiple CACCs forming process. The second conclusion can be found from figure 17 (d) and (e) that the spontaneous perturbation caused by controllers switching is amplified with multiple CACCs forming. However, the magnitude

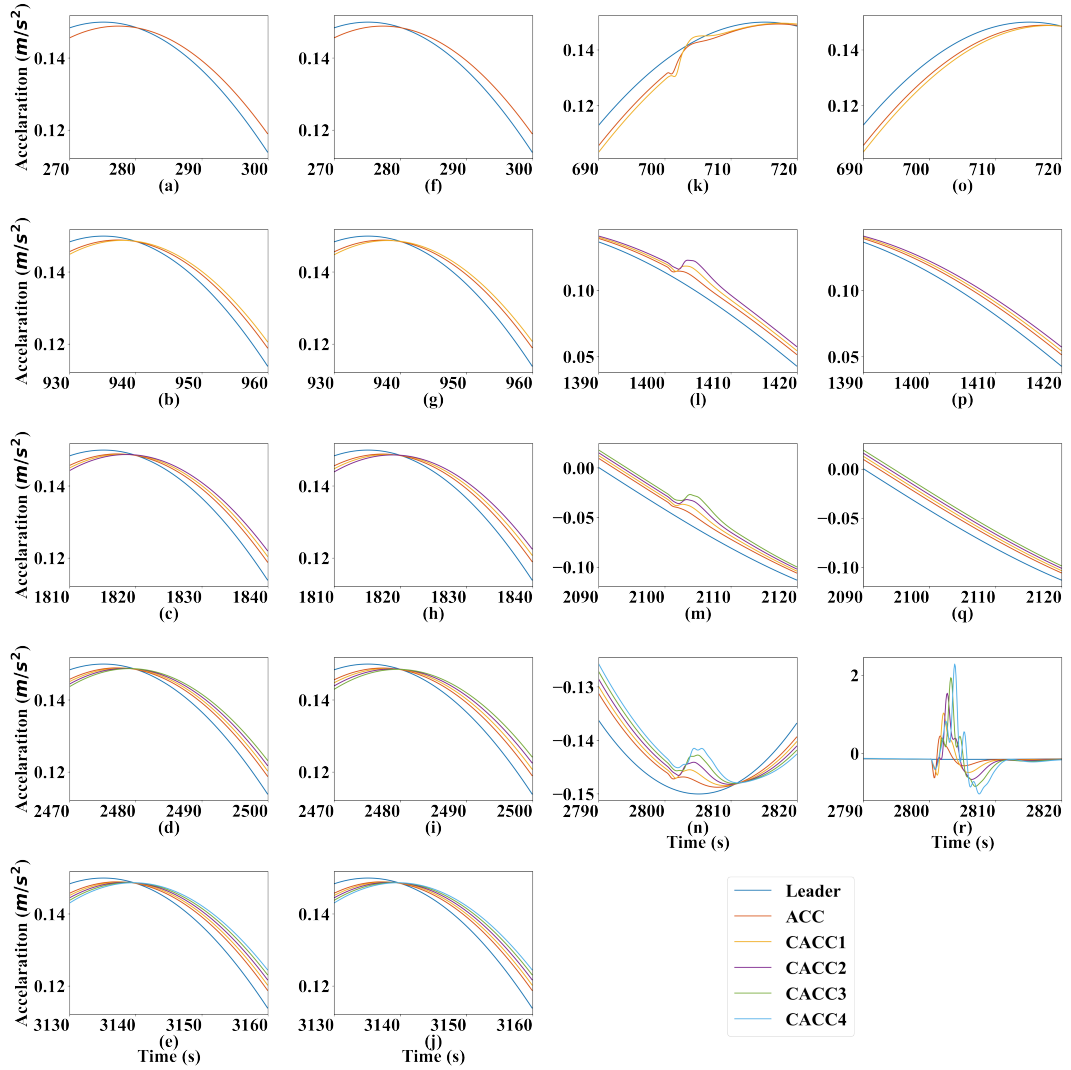


Figure 16: Detailed perturbation simulation results of experiment five and six: CACPC with or without YK parameterization under the fluctuating velocity case. For experiment five, (a)-(e) show the propagating processes of five applied perturbations and (k)-(l) show the four switching processes. For experiment six, (f)-(j) show the propagating processes of five applied perturbations and (o)-(r) show the four switching processes.

of the first switching perturbation is still only 0.015 m/s^2 which is significantly lower than the case without YK parameterization.

6. Conclusion

This paper proposes a control mode called CACPC to further improve the capacity by regarding the whole CACC platoon as the control object instead of a single vehicle. In this control mode, string stability of the CACC platoon is analyzed to get the margin desired time gap under different platoon sizes. Then YK parameterization is applied to ensure string stability of the CACC platoon when the CACC is switching from single vehicle control mode to platoon control mode, and the corresponding tuning function is proposed so that the specific platoon size does not limit the application range of this control mode. Moreover, the effectiveness of CACPC has been explored from two aspects: the impact of YK parameterization on dynamic performance of CACPC. The following conclusions can be drawn through this paper:

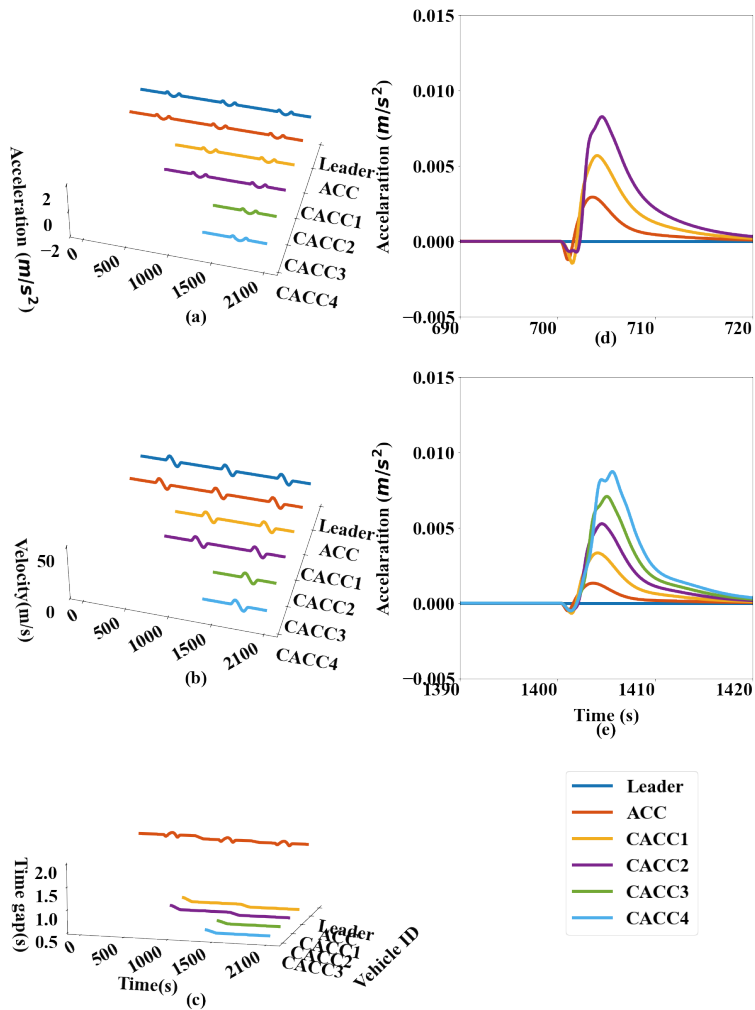


Figure 17: Simulation results of experiment seven: CACPC with YK parameterization under multiple CACCs forming at the same time. (a) Acceleration of simulation results; (b) Velocity of simulation results; (c) Time gap of simulation results; (d) Detailed acceleration of simulation results in 690-720s; (e) Detailed acceleration of simulation results in 1390-1420s

1. A new control mode is proposed to control the whole CACC platoon instead of a single vehicle.
2. CACPC is composed of two CACC controllers. YK parameterization ensures the stable interpolation between the two to guarantee smooth switching and string stability.
3. Combination of tuning function γ under different platoon sizes is derived by ensuring that the application range of CACPC is not limited by platoon size.
4. Adopting YK parameterization can significantly suppress the spontaneous perturbation from $2m/s^2$ to $0.015m/s^2$ caused by the controller switch.
5. YK parameterization can ensure smooth controller switching under the equilibrium state, traffic oscillation, and multiple CACCs forming.

Appendix A. System identification of lower level controller based on field experiments

Experiment preparation: The experiment was conducted at Closed test site of National Smart CAV & C-ITS (Beijing + Hebei) Demonstration Zone Shunyi Base on March 29, 2021. Two cycabs were used for experiment which were autonomous driving vehicles developed by iDriverplus technology company. The scheme of LiDAR+ millimeter



Figure 18: Field experiment scene.

wave + Ultrasonic radar + GPS inertial navigation was adopted as the navigation system, and the distance measurement accuracy is 0.05m. The decision frequency is 20 Hz which equals to a 50ms decision interval. The figure. 18 show the scene of the field experiment.

Experiment scheme: The experiments was divided into 5 groups. Each group had several rounds, which amounted to a total of 21 rounds of experiments. In each round, the front car drove in accordance with the speed configuration while the back car used the longitudinal control of ACC system to follow the front car and recorded the actual acceleration of the back car. Different groups used different control parameters of ACC system to ensure that a general conclusion can be drawn.

The control parameters of ACC system in different experiment groups are as follows:

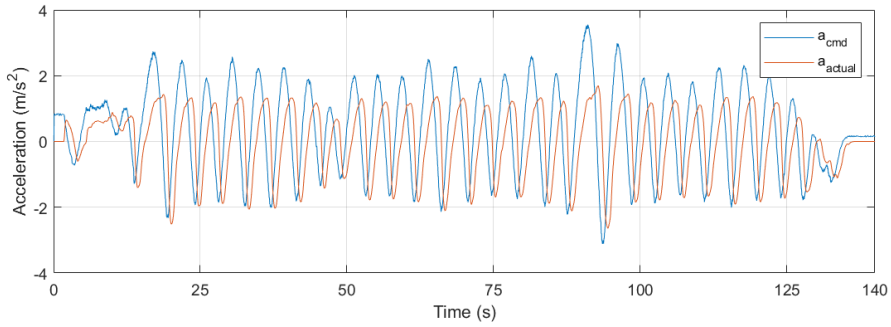
The experiment data of command acceleration and actual acceleration in first round are shown in figure. 19, where a_{cmd} means the command acceleration and a_{actual} means the actual acceleration.

In order to calibrate the transfer function of the lower controller $G_s(s)$, the command acceleration and actual acceleration of the back car in each round are regarded as input and output respectively. Notice that since the output of the lower controller $G_s(s)$ in figure. 2 is position instead of acceleration, additional second-order integration is applied. Using the System Identification toolbox in MATLAB and setting desire system type, the transfer function is fitted as

Table 2

Parameters chosen for different experiment groups.

Index of experiments group	k_p	k_d	h_i	round
1 st	0.7s^{-2}	0s^{-1}	2 s	2
2 nd	0.5s^{-2}	0s^{-1}	1.8 s	5
3 rd	0.6s^{-2}	0s^{-1}	2 s	7
4 th	0.7s^{-2}	0s^{-1}	2 s	4
5 th	0.4s^{-2}	0s^{-1}	2 s	3

**Figure 19:** Experiment data of the command acceleration and the actual acceleration in first round, where a_{cmd} means the command acceleration and a_{actual} means the actual acceleration.

follows:

$$G_i(s) = \frac{k_G}{s^2(\tau_i s + 1)} e^{-\phi_i s} = \frac{0.9403}{s^2(0.7862s + 1)} e^{-0.2s}, \quad (31)$$

which keeps fit error to minimum: FPE=0.08699 and MSE=0.0868.

Appendix B. Proof of the Equation (17-18)

The Equation (17-18) must satisfy the following identities:

- (a) $G = NM^{-1} = \tilde{M}^{-1}\tilde{N}$,
- (b) $K_i = U_i V_i^{-1} = \tilde{V}_i^{-1}\tilde{U}_i$,
- (c) $\begin{bmatrix} \tilde{V}_i & -\tilde{U}_i \\ -\tilde{N} & \tilde{M} \end{bmatrix} \begin{bmatrix} M & U_i \\ N & V_i \end{bmatrix} = \begin{bmatrix} M & U_i \\ N & V_i \end{bmatrix} \begin{bmatrix} \tilde{V}_i & -\tilde{U}_i \\ -\tilde{N} & \tilde{M} \end{bmatrix} = \begin{bmatrix} I & 0 \\ 0 & I \end{bmatrix}$.

Proof. Proof of (a) $G = \tilde{M}^{-1}\tilde{N}$:

$$\begin{aligned}
\tilde{M}^{-1}\tilde{N} &= \left[\begin{array}{cc|c} A + BD_i^c C & BC_i^c & BD_i^c \\ B_i^c C & A_i^c & B_i^c \\ \hline C & -F_i^c & I \end{array} \right]^{-1} \left[\begin{array}{cc|c} A + BD_i^c C & BC_i^c & B \\ B_i^c C & A_i^c & 0 \\ \hline C & -F_i^c & 0 \end{array} \right] \\
&= \left[\begin{array}{cc|c} A & B(C_i^c + D_i^c F_i^c) & -BD_i^c \\ 0 & A_i^c + B_i^c F_i^c & -B_i^c \\ \hline C & -F_i^c & I \end{array} \right] \left[\begin{array}{cc|c} A + BD_i^c C & BC_i^c & B \\ B_i^c C & A_i^c & 0 \\ \hline C & -F_i^c & 0 \end{array} \right] \\
&= \left[\begin{array}{cc|c} A & B(C_i^c + D_i^c F_i^c) & -BD_i^c C & BD_i^c F_i^c & 0 \\ 0 & A_i^c + B_i^c F_i^c & -B_i^c C & B_i^c F_i^c & 0 \\ 0 & 0 & A + BD_i^c C & BC_i^c & B \\ 0 & 0 & B_i^c C & A_i^c & 0 \\ \hline C & -F_i^c & C & -F_i^c & 0 \end{array} \right] \\
&= \left[\begin{array}{cc|c} A & B(C_i^c + D_i^c F_i^c) & 0 & 0 & B \\ 0 & A_i^c + B_i^c F_i^c & 0 & 0 & 0 \\ 0 & 0 & A + BD_i^c C & BC_i^c & B \\ 0 & 0 & B_i^c C & A_i^c & 0 \\ \hline C & -F_i^c & 0 & 0 & 0 \end{array} \right] \\
&= \left[\begin{array}{c|c} A & B \\ C & 0 \\ \hline C & 0 \end{array} \right], \tag{32}
\end{aligned}$$

where $\mathbf{T} = \begin{bmatrix} \mathbf{I} & 0 & -\mathbf{I} & 0 \\ 0 & \mathbf{I} & 0 & -\mathbf{I} \\ 0 & 0 & \mathbf{I} & 0 \\ 0 & 0 & 0 & \mathbf{I} \end{bmatrix}$, $\mathbf{T}^{-1} = \begin{bmatrix} \mathbf{I} & 0 & \mathbf{I} & 0 \\ 0 & \mathbf{I} & 0 & \mathbf{I} \\ 0 & 0 & \mathbf{I} & 0 \\ 0 & 0 & 0 & \mathbf{I} \end{bmatrix}$ is adopted in the similarity transformation. The proofs that $G = NM^{-1}$ and (ii) are analogous.

Proof. Proof of (c) $\begin{bmatrix} M & U_i \\ N & V_i \end{bmatrix} \begin{bmatrix} \tilde{V}_i & -\tilde{U}_i \\ -\tilde{N} & \tilde{M} \end{bmatrix} = \begin{bmatrix} I & 0 \\ 0 & I \end{bmatrix}$.

$$\begin{aligned}
&\left[\begin{array}{cc} M & U_i \\ N & V_i \end{array} \right]^{-1} \\
&= \left[\begin{array}{cc|c} A + BF & 0 & -B & 0 \\ 0 & A_i^c + B_i^c F_i^c & 0 & B_i^c \\ \hline -F & C_i^c + D_i^c F_i^c & I & D_i^c \\ -C & F_i^c & 0 & I \end{array} \right]^{-1} \\
&= \left[\begin{array}{cc|c} A + BD_i^c C & BC_i^c & -B & BD_i^c \\ B_i^c C & A_i^c & 0 & B_i^c \\ \hline F_i - D_i^c C & -C_i^c & I & -D_i^c \\ C & -F_i^c & 0 & I \end{array} \right] \\
&= \left[\begin{array}{cc} \tilde{V}_i & -\tilde{U}_i \\ -\tilde{N} & \tilde{M} \end{array} \right]. \tag{33}
\end{aligned}$$

Q.E.D.

CRediT authorship contribution statement

Hao Wang: Conceptualization of this study, Formal analysis, Funding acquisition, Supervision, Writing - review & editing. **Tiancheng Ruan:** Methodology, Writing - Original draft preparation, Resources, Software. **Linjie Zhou:** Data curation, Investigation. **YuXuan Hou:** Formal analysis, Writing - Original draft preparation. **Rui Jiang:** Data curation, Writing - review & editing.

Acknowledgment

This research was sponsored by the National Key Research and Development Program of China (No. 2019YFB1600200), National Science Foundation of China (No. 51878161, No. 71931002 and No.52072067).

References

- Bansal, P., Kockelman, K.M., 2017. Forecasting Americans' long-term adoption of connected and autonomous vehicle technologies. *Transportation Research Part A: Policy and Practice* 95, 49–63.
- Bian, Y., Zheng, Y., Ren, W., Li, S.E., Wang, J., Li, K., 2019. Reducing time headway for platooning of connected vehicles via v2v communication. *Transportation Research Part C: Emerging Technologies* 102, 87–105.
- Darbha, S., 2003. On the synthesis of controllers for continuous time LTI systems that achieve a non-negative impulse response. *Automatica* 39, 159–165.
- Dasgupta, S., Anderson, B.D., 1996. A parametrization for the closed-loop identification of nonlinear time-varying systems. *Automatica* 32, 1349–1360.
- Dey, K.C., Yan, L., Wang, X., Wang, Y., Shen, H., Chowdhury, M., Yu, L., Qiu, C., Soundararaj, V., 2015. A review of communication, driver characteristics, and controls aspects of cooperative adaptive cruise control (cacc). *IEEE Transactions on Intelligent Transportation Systems* 17, 491–509.
- Feng, S., Zhang, Y., Li, S.E., Cao, Z., Liu, H.X., Li, L., 2019. String stability for vehicular platoon control: Definitions and analysis methods. *Annual Reviews in Control* 47, 81–97.
- Gong, S., Du, L., 2018. Cooperative platoon control for a mixed traffic flow including human drive vehicles and connected and autonomous vehicles. *Transportation research part B: methodological* 116, 25–61.
- Jin, I.G., Orosz, G., 2014. Dynamics of connected vehicle systems with delayed acceleration feedback. *Transportation Research Part C: Emerging Technologies* 46, 46–64.
- Mahtout, I., Navas, F., Milanes, V., Nashashibi, F., 2020. Advances in youla-kucera parametrization: A review. *Annual Reviews in Control* 49, 81–94.
- Milanés, V., Shladover, S.E., 2014. Modeling cooperative and autonomous adaptive cruise control dynamic responses using experimental data. *Transportation Research Part C: Emerging Technologies* 48, 285–300.
- Milanés, V., Shladover, S.E., Spring, J., Nowakowski, C., Kawazoe, H., Nakamura, M., 2013. Cooperative adaptive cruise control in real traffic situations. *IEEE Transactions on intelligent transportation systems* 15, 296–305.
- Montanino, M., Monteil, J., Punzo, V., 2021. From homogeneous to heterogeneous traffic flows: Lp string stability under uncertain model parameters. *Transportation Research Part B: Methodological* 146, 136–154.
- Montanino, M., Punzo, V., 2021. On string stability of a mixed and heterogeneous traffic flow: A unifying modelling framework. *Transportation Research Part B: Methodological* 144, 133–154.
- Naus, G.J., Vugts, R.P., Ploeg, J., van De Molengraft, M.J., Steinbuch, M., 2010. String-stable cacc design and experimental validation: A frequency-domain approach. *IEEE Transactions on vehicular technology* 59, 4268–4279.
- Navas, F., Milanés, V., 2019. Mixing v2v-and non-v2v-equipped vehicles in car following. *Transportation research part C: emerging technologies* 108, 167–181.
- Navas, F., Milanés, V., Nashashibi, F., 2016. Using plug&play control for stable acc-cacc system transitions, in: 2016 IEEE Intelligent Vehicles Symposium (IV), IEEE. pp. 704–709.
- Navas, F., Milanés, V., Nashashibi, F., 2017. Youla-kucera based online closed-loop identification for longitudinal vehicle dynamics, in: 2017 21st International Conference on System Theory, Control and Computing (ICSTCC), IEEE. pp. 88–93.
- Niemann, H., Stoustrup, J., 1999. An architecture for implementation of multivariable controllers, in: Proceedings of the 1999 American Control Conference (Cat. No. 99CH36251), IEEE. pp. 4029–4033.
- Oncu, S., Ploeg, J., Van De Wouw, N., Nijmeijer, H., 2014. Cooperative adaptive cruise control: Network-aware analysis of string stability. *IEEE Transactions on Intelligent Transportation Systems* 15, 1527–1537. doi:10.1109/TITS.2014.2302816.
- Orosz, G.b., Moehlis, J., Bullo, F., 2011. Delayed car-following dynamics for human and robotic drivers, in: International Design Engineering Technical Conferences and Computers and Information in Engineering Conference, pp. 529–538.
- Ploeg, J., Scheepers, B.T., Van Nunen, E., Van de Wouw, N., Nijmeijer, H., 2011. Design and experimental evaluation of cooperative adaptive cruise control, in: 2011 14th International IEEE Conference on Intelligent Transportation Systems (ITSC), IEEE. pp. 260–265.
- Ploeg, J., Van De Wouw, N., Nijmeijer, H., 2013. Lp string stability of cascaded systems: Application to vehicle platooning. *IEEE Transactions on Control Systems Technology* 22, 786–793.
- Pommaret, J., Quadrat, A., 1998. Generalized bezout identity. *Applicable Algebra in Engineering, Communication and Computing* 9, 91–116.
- Qin, Y., Wang, H., 2021. Analytical framework of string stability of connected and autonomous platoons with electronic throttle angle feedback. *Transportmetrica A: Transport Science* 17, 59–80.
- Qin, Y., Wang, H., Ran, B., 2018. Stability analysis of connected and automated vehicles to reduce fuel consumption and emissions. *Journal of Transportation Engineering, Part A: Systems* 144, 04018068.
- Ruan, T., Zhou, L., Wang, H., 2021. Stability of heterogeneous traffic considering impacts of platoon management with multiple time delays. *Physica A: Statistical Mechanics and its Applications* 583, 126294.
- Stüdli, S., Seron, M.M., Middleton, R.H., 2017. From vehicular platoons to general networked systems: String stability and related concepts. *Annual Reviews in Control* 44, 157–172. doi:10.1016/j.arcontrol.2017.09.016.
- Sun, J., Zheng, Z., Sun, J., 2018. Stability analysis methods and their applicability to car-following models in conventional and connected environments. *Transportation research part B: methodological* 109, 212–237.

- Swaroop, D., 1994. String stability of interconnected systems: An application to platooning in automated highway systems.
- Tay, T.T., Mareels, I., Moore, J.B., 1998. High performance control. Springer Science & Business Media.
- Wang, C., Gong, S., Zhou, A., Li, T., Peeta, S., 2020. Cooperative adaptive cruise control for connected autonomous vehicles by factoring communication-related constraints. *Transportation Research Part C: Emerging Technologies* 113, 124–145.
- Wang, M., 2018. Infrastructure assisted adaptive driving to stabilise heterogeneous vehicle strings. *Transportation Research Part C: Emerging Technologies* 91, 276–295.
- Wang, Z., Bian, Y., Shladover, S.E., Wu, G., Li, S.E., Barth, M.J., 2019. A survey on cooperative longitudinal motion control of multiple connected and automated vehicles. *IEEE Intelligent Transportation Systems Magazine* 12, 4–24.
- Xiao, L., Gao, F., 2011. Practical string stability of platoon of adaptive cruise control vehicles. *IEEE Transactions on intelligent transportation systems* 12, 1184–1194.
- Zhang, Y., Bai, Y., Hu, J., Wang, M., 2020. Control design, stability analysis, and traffic flow implications for cooperative adaptive cruise control systems with compensation of communication delay. *Transportation Research Record* 2674, 638–652.
- Zhou, L., Ruan, T., Ma, K., Dong, C., Wang, H., 2021. Impact of cav platoon management on traffic flow considering degradation of control mode. *Physica A: Statistical Mechanics and its Applications* , 126193.
- Zhou, Y., Ahn, S., Wang, M., Hoogendoorn, S., 2020. Stabilizing mixed vehicular platoons with connected automated vehicles: An h-infinity approach. *Transportation Research Part B: Methodological* 132, 152–170.